Industrial Radio Link Abstraction Models for Short Packet Communication with Polar Codes

Johannes Demel, Carsten Bockelmann, Armin Dekorsy
Department of Communications Engineering
University of Bremen
Bremen, Germany
Email: {demel,bockelmann,dekorsy}@ant.uni-bremen.de

***Abstract*—Industrial radio communication systems spawn a new set of requirements for wireless communication systems with high reliability and low latency. These requirements were identified in the Industry 4.0 (I4.0) initiative as well as in 5th Generation (5G) mobile communication standardization where polar codes are selected to meet Ultra Reliable Low Latency Communication (URLLC) requirements. Accurate link abstraction models of those systems are required for system level simulations. However, it is uncertain how short, polar-coded packets with Bit-Interleaved Coded Mapping (BICM) in Orthogonal Frequency Division Multiplexing (OFDM) systems at low Frame-Error-Rates (FERs) can be characterized via Effective SNR Mapping (ESM). We investigate if and how short packet communication systems with polar codes can be modeled accurately via ESM methods. We compare new error measures for FER curve fitting in order to find optimal ESM adjustment factors for low FERs. We present simulation results that show how susceptible adjustment factors are to different system parameters. Finally, we demonstrate that accurate link abstraction is possible for the target system even at the desired working point.**

***Index Terms*—polar code, EESM, MIESM, link abstraction, effective SNR mapping, multicarrier, URLLC, 5G**

I. Introduction

In 5th Generation (5G) Ultra Reliable Low Latency Communication (URLLC) new use cases for Machine-type-Communication (MTC) systems are identified [1]. The 3rd Generation Partnership Project (3GPP) considers polar codes for these use cases [2] which include industrial systems and autonomous driving. Here, high reliability requirements paired with low latency constraints complicate satisfactory communication system design. 5G communication systems aim at providing the Quality-of-Service (QoS) requirements for reliable and low latency communications for future mobile communication scenarios [3].

Industrial communication systems may consist of tens or hundreds of devices. Furthermore, they pose a new set of requirements with highly reliable short packets, low latency and resilience to burst errors. Communication engineers often use Frame-Error-Rate (FER) to compare system performance while automation engineers use Mean Time To Failure (MTTF) as their Key Performance Indicator (KPI) [4]. In [4] the authors proposed a method to obtain a relation between those KPIs and showed that automation systems require extremely low FERs which may lead to high resource consumption but do not directly address resilience to burst errors.

We need accurate link abstraction models to find and analyze new scheduling and resource allocation algorithms to target these system requirements [5]. These models need to take into account the physical constraints and shall deliver a simple link characterization, preferably a simple FER [6]. Otherwise accurate system level simulations need to simulate the whole PHYsical layer (PHY) instead of employing a simple, accurate link abstraction model. In this case system simulation complexity would be too high. However, it is uncertain how short packet PHY system design according to URLLC principles can be accurately abstracted with Effective SNR Mapping (ESM) approaches. We investigate if and how ESM approaches can be used for URLLC systems with short packets.

Recently polar codes were adopted for 5G mobile communication systems [2]. Especially control channels and URLLC are anticipated use cases for polar codes. Since their initial publication, polar codes received a huge amount of attention [7]–[10]. Also, different approaches to adapt polar codeword lengths through puncturing and shortening are known in literature [11]–[13]. Here, we point out which methods are preferable according to our findings. Previous studies on polar codes in Rayleigh fading setups only consider frequency flat channels [14]. We study polar codes in frequency selective block fading channels with Orthogonal Frequency Division Multiplexing (OFDM) modulation [15]. Thus, channel gains may vary over different subcarriers which justifies a Bit-Interleaved Coded Mapping (BICM) approach to take advantage of diversity [16].

Our main contribution is an investigation if and how link abstraction via ESM techniques can be applied to polar code systems with short packets and low FER requirements. We evaluate error measures to find optimal adjustment factors for ESM methods. Typically, Mean Square Error (MSE) is used as an error measure [6] but according to our findings this neglects small FER values which are of special interest for industrial radio systems. Thus, we propose a relative error measure to find optimal adjustment factors. Furthermore, we run a simulation campaign to explore the impact of different system parameters on optimal adjustment factors. Finally, we discuss how adjustment factors can be used to represent systems for a range of varying parameters.

II. Theory

In this section we briefly describe the theoretical background of our work. The interested reader may refer to references given in this section for a deeper discussion on specific topics. The described system serves as a foundation for our link abstraction investigations afterwards. In Fig. 1 the transmitter signal processing chain for the system under consideration is shown. First, a polar code for Forward Error Correction (FEC) is applied, then codewords are punctured, afterwards codebits are interleaved and finally mapped to complex symbols.

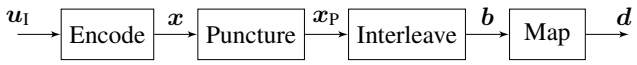

Fig. 1. Schematic of the transmitter chain for our ESM evaluations

A. Polar Codes

Polar Codes are first presented in [7]. Here, we want to summarize prior research that is relevant to our work. We consider symmetric binary input $\mathbb{B} = \{0, 1\}$ over a Discrete Memoryless Channel (DMC), such as a Binary Erasure Channel (BEC), Binary Symmetric Channel (BSC) or Additive White Gaussian Noise (AWGN) channel [17]. First, we consider a bit vector $\boldsymbol{u} \in \mathbb{B}^2$ of size 2. $\boldsymbol{u}$ is combined into the codeword $\boldsymbol{x} \in \mathbb{B}^2$ by

$$\boldsymbol{x} = \boldsymbol{u}\boldsymbol{F} \quad \text{with} \quad \boldsymbol{F} = \begin{pmatrix} 1 & 0 \\ 1 & 1 \end{pmatrix} \tag{1}$$

over GF(2) and transmitted via two channel uses. Then, we extend this scheme to bit vectors $\boldsymbol{u} \in \mathbb{B}^N$ of size $N = 2^n$. We obtain the codeword for transmission by

$$\boldsymbol{x} = \boldsymbol{u} \cdot \boldsymbol{B}_N \cdot \boldsymbol{G} \quad \text{with} \quad \boldsymbol{G} = \boldsymbol{F}^{\otimes n} \tag{2}$$

where $\boldsymbol{B}_N$ is a bit reversal matrix. Without $\boldsymbol{B}_N$ the obtained codeword is in bit-reversed order while with $\boldsymbol{B}_N$ it is in natural bit order [7], [18]. $\boldsymbol{F}^{\otimes n}$ is the nth Kronecker product which is defined recursively as

$$\boldsymbol{F}^{\otimes n} = \begin{pmatrix} \boldsymbol{F}^{\otimes (n-1)} & \boldsymbol{0} \\ \boldsymbol{F}^{\otimes (n-1)} & \boldsymbol{F}^{\otimes (n-1)} \end{pmatrix} \quad \text{with} \quad \boldsymbol{F}^{\otimes 1} = \boldsymbol{F} \tag{3}$$

The bit vector $\boldsymbol{u}$ consists of so called frozen bits $\boldsymbol{u}_\mathrm{Fr} \in \boldsymbol{0}^{N-K}$ and information bits $\boldsymbol{u}_\mathrm{I} \in \mathbb{B}^K$. The set of frozen bit positions $\mathcal{A}_\mathrm{Fr}$, with $|\mathcal{A}_\mathrm{Fr}| = N - K$, in a bit vector $\boldsymbol{u}$ is determined via polar channel construction. Polar codes are then defined as $(N, K, \mathcal{A}_\mathrm{Fr})$ codes.

We refer to [10] and references therein for an in-depth discussion on possible strategies to obtain frozen bit positions $\mathcal{A}_\mathrm{Fr}$. In general, the discussed encoder together with a soon-to-be-discussed Successive Cancellation (SC) decoder are used to obtain virtual or synthetic bit channels. The capacities of these virtual bit channels tends to be either 0 or 1. The goal of channel construction is to calculate these N capacities depending on a design-SNR which represents the target working point. Then, we select the K best channels for information bits while the others are frozen bits. We opt for the Bhattachryya Bounds method because of its simplicity and good performance.

Originally, Arıkan proposed a SC decoder to prove that polar codes achieve capacity. Here, we explain the decoding process for $N = 2$. This may be recursively extended for longer polar codes [7], [19]. A receiver calculates Log-Likelihood Ratios (LLRs)

$$L(y_i) = \ln \frac{p(x_i = 0|y_i)}{p(x_i = 1|y_i)} \tag{4}$$

for each received symbol y_i where $p(x_i|y_i)$ is the conditional probability density function. Now, for $L(u_0)$ we calculate

$$L(u_0) = L(y_0) \boxplus L(y_1) \tag{5}$$

and perform hard decision with $u_0 = 0$ for $L(u_0) > 0$ and $u_0 = 1$ otherwise. The $\boxplus$ operator is defined as $c = a \boxplus b = \log \frac{1+e^a e^b}{e^a+e^b} \approx \operatorname{sgn}(a)\operatorname{sgn}(b)\min(|a|, |b|)$. If $0 \in \mathcal{A}_\mathrm{Fr}$ then u_0 is a frozen bit and we decide for its known frozen bit value, mostly $u_0 = 0$.

In order to decode u_1, we calculate

$$L(u_1) = L(y_0) + (-1)^{u_0} L(y_1) \tag{6}$$

and again we make a hard decision afterwards. This SC decoder may be optimized to the Fast Simplified Successive Cancellation (Fast-SSC) decoder in order to improve throughput and reduce latency [19]. For the remainder of this work, we restrict ourselves to SC decoders in order to obtain a good baseline.

Non-systematic polar codes were modified to systematic polar codes [20], [21]. Systematic Polar Codes exhibit the same complexity as non-systematic Polar Codes. Though, the structure of the code vector $\boldsymbol{x}$ differs slightly such that $\boldsymbol{u}_\mathrm{I} = \boldsymbol{x}_{\mathcal{A}_\mathrm{I}}$ while there are parity bits $\boldsymbol{x}_{\mathcal{A}_\mathrm{Fr}}$ at the other indices.

B. Puncturing

Polar code codeword sizes are inherently restricted to a power of 2. We circumvent this obstacle by puncturing or shortening strategies [13], though we need to carefully choose a puncturing pattern otherwise code performance may be degraded dramatically [12]. First, we find a mother codeword length $N = 2^{\lceil \log_2 N_\mathrm{P} \rceil}$ to a desired punctured codeword length N_P. Then, we puncture the codeword $\boldsymbol{x}$ at the $P = N - N_\mathrm{P}$ most suitable indices in order to obtain the punctured codeword $\boldsymbol{x}_\mathrm{P} \in \mathcal{B}^{N_\mathrm{P}}$.

The authors in [11] proposed Quasi Uniform Puncturing (QUP) for non-systematic polar codes. The QUP puncturing positions are obtained by bit-reversing the first P vector indices. Systematic polar codes do not require bit-reversal. In [12] it was recognized that only frozen bit positions, or their bit-reversed positions, are eligible puncturing positions. Thus, instead of the first P vector indices, we use Frozen-QUP, i.e. we use the first P frozen bit indices as puncturing positions. The authors in [12] proposed to choose P puncturing positions which correspond to virtual bit channels with minimum reliability. Alternatively, we can randomly draw puncturing positions among the frozen bit positions.

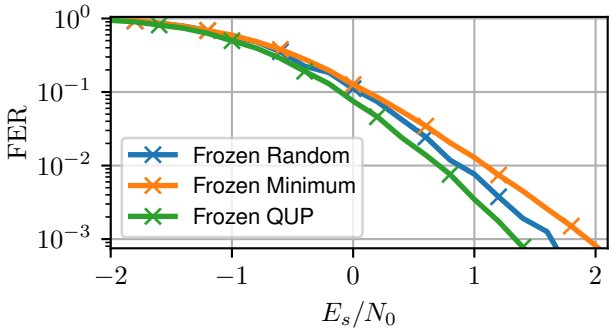

Fig. 2. FERs for different puncturing schemes for $(768, 256)$ polar codes.

FERs over AWGN for the different puncturing schemes for systematic polar codes are shown in Fig. 2. Here, we conclude that Frozen-QUP yields the lowest FER and thus we restrict ourselves to this puncturing scheme. The random puncturing scheme shows slightly erratic behavior because we obtained a new set of puncturing positions for each simulation point.

C. Bit-Interleaved Coded Mapping

We combine polar codes with BICM in order to leverage diversity [16]. We employ a standard random interleaver in order to obtain an interleaved bit vector $\boldsymbol{b} \in \mathcal{B}^{N_\mathrm{P}}$ from a punctured codeword $\boldsymbol{x}_\mathrm{P}$.

Then, groups of constellation order size M from $\boldsymbol{b}$ are uniquely mapped to complex symbols according to the desired alphabet. Here, Gray labeling is assumed in order to optimize the distance between symbols. In our work, we use Binary Phase Shift Keying (BPSK), Quadrature Phase Shift Keying (QPSK), 8-Phase Shift Keying (PSK) and 16-Quadrature Amplitude Modulation (QAM) alphabets $\mathcal{A}$, $|\mathcal{A}| = 2^M$. For the sake of simplicity we assume the mean signal energy to be $\sigma_d^2 = E\{|d|^2\} = 1$. Thus, we obtain the transmit vector $\boldsymbol{d} \in \mathbb{C}^{N_\mathrm{s}}$ with $N_\mathrm{s} = N_\mathrm{P}/M$ elements. We can now define the effective rate

$$R_{eff} = \frac{M \cdot K}{N_\mathrm{P}} \tag{7}$$

as the mean amount of information conveyed by each transmitted symbol in $\boldsymbol{d}$.

III. Modulation and Channel Model

In this section we present our OFDM channel model [15]. A frame $\boldsymbol{d}$ is OFDM modulated, transmitted over a frequency selective Rayleigh block fading channel and affected by AWGN. At the receiver, after demodulation and channel equalization, we obtain the received frame $\hat{\boldsymbol{d}}$ for further receive processing. The equivalent frequency domain channel model can be written as

$$\hat{\boldsymbol{d}} = \boldsymbol{G}\left(\boldsymbol{H}\boldsymbol{d} + \boldsymbol{n}\right) \tag{8}$$

where $n_i \in \mathcal{CN}(0, \sigma_n^2)$ are the complex Gaussian distributed noise elements of the noise vector $\boldsymbol{n}$. Thus, we denote Signal-to-Noise-Ratio (SNR) as $E\{|d|^2\}/E\{|n|^2\} = E_s/N_0 = \sigma_d^2/\sigma_n^2$. The channel matrix $\boldsymbol{H} \in \mathcal{C}^{N_\mathrm{s} \times N_\mathrm{s}}$ is a diagonal matrix, i.e. all off-diagonal elements are zero. This implies that each received symbol is transmitted over a frequency flat subcarrier channel plus noise. The distribution of the complex diagonal elements h_i is assumed to be $\mathcal{CN}(0, 1)$. $\boldsymbol{G}$ is an equalizer matrix and will be discussed in Sec. III-A.

This channel model relies on several assumptions. The channel is constant over the transmit duration of one frame. The Cyclic Prefix (CP) duration τ_CP is assumed to be larger than the maximum channel delay τ_max. Furthermore, we assume perfect system synchronization, i.e. we assume zero time and frequency offsets. If a frame $\boldsymbol{d}$ has more than N_FFT elements, it is transmitted over multiple OFDM symbols. With the block fading assumption, symbols transmitted in the same frame on the ith subcarrier are affected by the same channel tap h_i.

A. Equalization strategies

At the receiver we need to mitigate channel distortions. With the discussed channel assumptions, we can narrow down the choice of equalizers to a simple one-tap Matched-Filter (MF) or Minimum Mean Square Error (MMSE) equalizer for each subcarrier [15]. In other words, the equalizer matrix $\boldsymbol{G}$ is a diagonal matrix with g_i as its diagonal elements.

For symbol alphabets $\mathcal{A}$ which solely use phase to carry information we use MF $g_{\mathrm{MF},i} = h_i^*$ where * denotes complex conjugation. The MF approach is ideal in the sense that it maximizes SNR. Though, for alphabets which use amplitude to carry information the MF approach adds additional distortion.

With the MMSE approach, we try to find an equilibrium between SNR maximization and amplitude distortion. This leads to $g_{\mathrm{MMSE},i} = (h_i^* h_i + \sigma_n^2)^{-1} h_i^*$ for equalization. This approach allows to equalize alphabets such as 16-QAM.

B. In-depth channel assumptions

Ongoing measurement campaigns within project HiFlecs and other industrial radio projects show that all time-domain channel taps $\tilde{h}_i$, regardless if they are Line-Of-Sight (LOS) or Non-Line-Of-Sight (NLOS), are Rayleigh distributed. Also, the Power Delay Profile (PDP) $\boldsymbol{p}$ of the channel follows an exponential distribution with a delay spread σ_RMS in the range $40\,\mathrm{ns}$ to $100\,\mathrm{ns}$. Typically the maximum channel delay τ_max varies around $200\,\mathrm{ns}$. We obtain the ith channel tap by $\tilde{h}_i = p_i \cdot \tilde{h}_{\mathrm{R},i}$, $\tilde{h}_{\mathrm{R},i} \in \mathcal{CN}(0, 1)$. Finally, frequency-domain channel taps are obtained as $\boldsymbol{h} = \mathcal{F}_N \tilde{\boldsymbol{h}}$.

We focus on short packets, thus we assume a block fading channel, i.e. the channel is constant over the duration of a frame. The channel covariance ρ for consecutive frames can be approximated as

$$\rho = \exp\left\{-23 \cdot \left(\frac{\Delta t v f_c}{c_0}\right)^2\right\} \tag{9}$$

depending on time difference Δt, carrier frequency f_c and relative velocity v between transmitter and receiver [22]. Channel covariance ρ quantifies how statistically dependent consecutive channel realizations are, i.e. $\rho = 1$ indicates that the channel did not change at all.

IV. Link abstraction

Usually, link abstraction is facilitated by transforming per-subcarrier Carrier-to-Noise-Ratios (CNRs)

$$\mathrm{CNR}_i = \frac{|h_i|^2 \sigma_d^2}{\sigma_n^2} \tag{10}$$

for all occupied subcarriers into an effective Signal-to-Noise-Ratio $\mathrm{SNR}_{\mathrm{eff}}$ equivalent to the AWGN simulation results as shown in Fig. 3. We can obtain the final FER from AWGN FER curves, as shown in Fig. 6, with the calculated effective SNR. The methodology is to run extensive simulations for all desired Modulation and Coding Scheme (MCS) with the described channel model and then find a suitable translation into effective SNR and further into a FER [23].

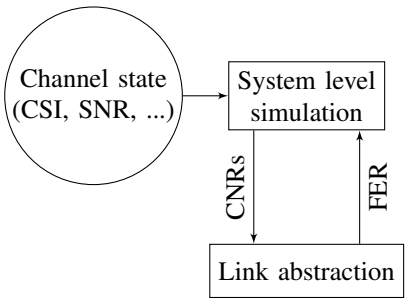

Fig. 3. Link abstraction concept

A. Effective SNR Mapping

The process of converting Channel State Information (CSI) into an effective SNR is called Effective SNR Mapping (ESM). We evaluate two different methods for ESM, namely Mutual Information Effective SNR Mapping (MIESM) and Exponential Effective SNR Mapping (EESM) [23]. The chosen approach is described in [6].

For EESM and MIESM per-subcarrier CNRs are used to calculate

$$\mathrm{SNR}_{\mathrm{eff}} = \beta I^{-1}\left(\frac{1}{N_{\mathrm{FFT}}}\sum_{i=0}^{N_{\mathrm{FFT}}-1} I\left(\frac{\mathrm{CNR}_i}{\beta}\right)\right) \tag{11}$$

where the function $I(\dots)$ is chosen according to the desired method for EESM or MIESM and β is an adjustment factor, discussed in Sec. IV-B [6]. We assume that N_{FFT} subcarriers are occupied. For EESM we effectively calculate

$$\mathrm{SNR}_{\mathrm{eff}} = -\beta \ln\left(\frac{1}{N_{\mathrm{FFT}}}\sum_{i=0}^{N_{\mathrm{FFT}}-1} \exp\left(-\frac{\mathrm{CNR}_i}{\beta}\right)\right) \tag{12}$$

with the LogSumExp (LSE) algorithm for numerical stability.

The function $I(\dots)$ for MIESM depends on the chosen modulation alphabet $\mathcal{A}$. The mutual information I_{BICM} calculation for BICM is split into M different bit layers [24]. For each bit layer, we compute

$$I_{\mathrm{BICM},i} = 1 - \mathrm{E}_{b,y}\left\{\log_2 \frac{\sum_{d_2\in\mathcal{A}} p_{y|d}(y|d_2)}{\sum_{d_3\in\mathcal{A}_i^b} p_{y|d}(y|d_3)}\right\} \tag{13}$$

and then calculate $I_{\mathrm{BICM}} = \sum_{i=0}^{M-1} I_{\mathrm{BICM},i}$ for the desired SNR. $I_{\mathrm{BICM},i}$ can be rewritten into

$$I_{\mathrm{BICM},i} = 1 - \frac{1}{2M\pi} \cdot \sum_{b=0}^{1}\sum_{d_1\in\mathcal{A}} \int_{\mathbb{C}} e^{-|\zeta-d_1/\sigma_n|^2} \log_2 \frac{\sum_{d_2\in\mathcal{A}} e^{-|\zeta-d_2/\sigma_n|^2}}{\sum_{d_3\in\mathcal{A}_i^b} e^{-|\zeta-d_3/\sigma_n|^2}} \mathrm{d}\zeta \tag{14}$$

which is then calculated after further rearrangements via multivariate Gauss-Hermite-Quadrature with N_{GHQ} evaluation points per dimension [25]. The set $\mathcal{A}_i^b$ is comprised of all elements in $\mathcal{A}$ with bitmap value b at position i. Results for different modulations are shown in Fig. 4 together with Gaussian capacity. Computing these values is potentially a resource intensive task, thus we will use cached values in conjunction with linear interpolation.

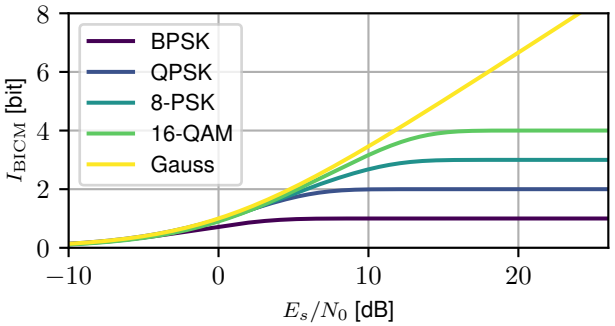

Fig. 4. Mutual Information over SNR with $N_{\mathrm{GHQ}} = 128$

B. Adjustment Factor Calibration

It is crucial to find a fitting adjustment factor β for each MCS which matches the calculated ESM values $\mathrm{FER}_{\mathrm{ESM}}^{\mathrm{MCS}}(\beta)$ to the AWGN values $\mathrm{FER}_{\mathrm{AWGN}}^{\mathrm{MCS}}$ [6]. Each $\mathrm{FER}_{\mathrm{AWGN}}^{\mathrm{MCS}}$ denotes a FER over SNR curve with N_{e} evaluation points over an AWGN channel. In order to obtain $\mathrm{FER}_{\mathrm{ESM}}^{\mathrm{MCS}}(\beta)$ for a given β it is necessary to recalculate $\mathrm{SNR}_{\mathrm{eff}}$ for all simulated frames. Then, we sort the results into bins in order to obtain the desired FER over $\mathrm{SNR}_{\mathrm{eff}}$ curves as $\mathrm{FER}_{\mathrm{ESM}}^{\mathrm{MCS}}(\beta)$. We chose the bin width for this sorting to be $0.1\,\mathrm{dB}$.

First, we obtain FER values $\mathrm{FER}_{\mathrm{AWGN}}^{\mathrm{MCS}}$ for all desired MCS over AWGN channels. Second, we run simulations for Rayleigh fading channels with $\approx 5 \cdot 10^6$ frames per MCS. Finally, we search for

$$\beta_{\mathrm{opt}}^{\mathrm{MCS}} = \underset{\beta}{\operatorname{argmin}}\, \epsilon(\beta) \tag{15}$$

which minimizes the error measure ϵ. The error measure denotes the deviation of the ESM FER curve from its AWGN counterpart for a given β.

Other works use MSE as an error measure. Our observation is that MSE neglects low FER values and thus we consider several alternatives. In Fig. 5 the resulting FER over effective

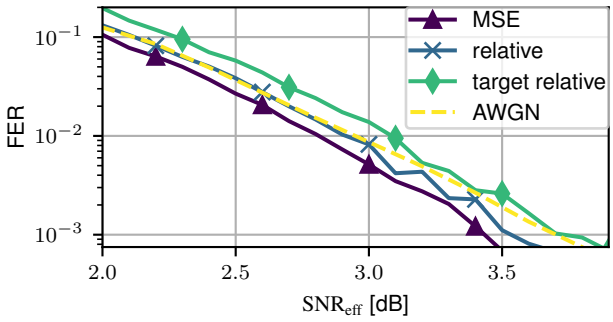

Fig. 5. FER curve results for different error measures ϵ.

SNR curves are shown and were obtained as described in Sec. V.

First, we consider a relative error measure

$$\epsilon_{\mathrm{rel}}(\beta) = \sum_{i=0}^{N_{\mathrm{e}}-1} \frac{\left|\mathrm{FER}^{\mathrm{MCS}}_{\mathrm{ESM},i}(\beta) - \mathrm{FER}^{\mathrm{MCS}}_{\mathrm{AWGN},i}\right|}{\mathrm{FER}^{\mathrm{MCS}}_{\mathrm{AWGN},i}} \tag{16}$$

where we assume that $\mathrm{SNR} = \mathrm{SNR}_{\mathrm{eff}}$ for each evaluation point i. Thus $\epsilon_{\mathrm{rel}}(\beta)$ quantifies the deviation from the AWGN reference FER curve. Second, we consider MSE as the error measure

$$\epsilon_{\mathrm{MSE}}(\beta) = \sum_{i=0}^{N_{\mathrm{e}}-1} \left|\mathrm{FER}^{\mathrm{MCS}}_{\mathrm{ESM},i}(\beta) - \mathrm{FER}^{\mathrm{MCS}}_{\mathrm{AWGN},i}\right|^2 \tag{17}$$

[6]. Third, we try to minimize the error measure for a target FER rate. Here, we calculate

$$\epsilon_t(\beta) = \left|\mathrm{FER}^{\mathrm{MCS}}_{\mathrm{ESM},t}(\beta) - \mathrm{FER}^{\mathrm{MCS}}_{\mathrm{AWGN},t}\right| \tag{18}$$

with t being an indicator for our target FER which we chose to be 10^{-3}. Thus, only one evaluation point is used in this case.

From Fig. 5 we observe that the MSE measure yields FER values which are too low compared to AWGN curve. While the target FER approach yields results which tend to be too high. The relative error measure comes out in between the other two approaches and tends to yield results very close to the AWGN error curve. Thus, we conclude that the relative error measure should be preferred to find suitable β values.

V. Numerical Evaluation

All AWGN reference simulation points are obtained by simulating at least 8192 frames and then continue to simulate frames until 1024 erroneous frames are detected for each SNR data point. For Rayleigh channel simulations we simulated $2^{19} = 524288$ frames for each data point, though again we use an early stop criterion with 8192 erroneous frames.

For all simulations we use the transmitter chain depicted in Fig. 1 with the channel as described in Sec. III. At the receiver, we assume perfect CSI and SNR knowledge. Our reference system is an OFDM system with $N_{\mathrm{FFT}} = 128$, a polar code with $(512, 256)$ and a design-SNR with $0\,\mathrm{dB}$. We use this setup for numerical evaluations and investigate how suitable the previously presented approaches are for ESM.

We want to find β_{opt} such that the FER over $\mathrm{SNR}_{\mathrm{eff}}$ curves match their FER over AWGN references shown in Fig. 6 as closely as possible. The results in Fig. 6 lead to the conclusion

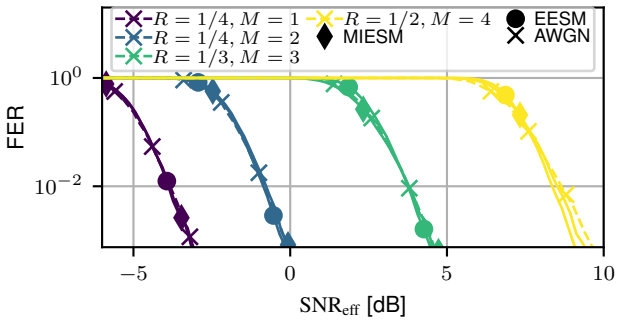

Fig. 6. FER over $\mathrm{SNR}/\mathrm{SNR}_{\mathrm{eff}}$ with $K = 256$.

that a β_{opt} that matches these curves can be found for the system under consideration.

In Fig. 6 we compare selected AWGN reference curves with their respective matched EESM and MIESM FER curves. Crosses indicate FER over SNR curves for AWGN channels. Diamonds and dots indicate FER over effective SNR curves for MIESM and EESM respectively. These curves are obtained with β_{opt} to calculate the effective SNR. Lower constellation orders and lower coderates result in a better match of these ESM to AWGN curves. It is possible to accurately match AWGN reference curves via the investigated link abstraction methods.

Next, we want to analyze how changing different system parameters impacts the adjustment factor β_{opt}. We are especially interested in how the number of subcarriers N_{FFT}, the coderate for constant block length and the code rate for constant information vector length affect the optimal β. Furthermore, we investigate the impact of the modulation order.

As expected, the number of subcarriers does not change the resulting β_{opt}. Thus, separate evaluations for systems with different numbers of subcarriers are not required. During our evaluations we assumed that it is sufficient to only use N_{FFT} evaluation points for ESM. This holds as long as N_{d} is a multiple of N_{FFT} otherwise special precautions need to be taken into account.

In Fig. 7 a comparison of EESM and MIESM adjustment factors β for different modulation orders is shown. We observe that MIESM β is robust against different constellation orders M while EESM β is susceptible to such a change. Since MIESM does explicitly account for the modulation order, this is to be expected. Finding β_{opt} is a complex and tedious task. Thus, we conclude it is advantageous to use MIESM because we can reduce the number of simulations. This leads to faster overall link abstraction because we can select a representative β_{opt} for multiple configurations.

In Fig. 8 we compare ϵ over β for different coderates for MIESM. The results for EESM are similar and thus we omit

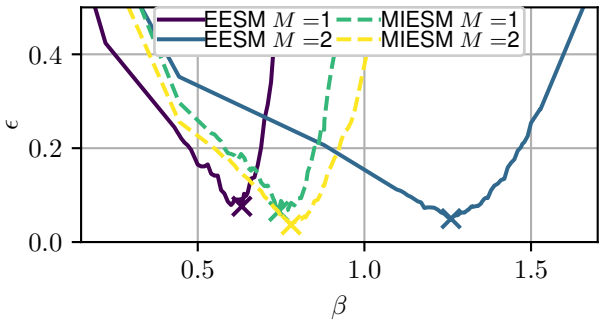

Fig. 7. ϵ over β for EESM and MIESM for different M with $N = 512$, $K = 256$.

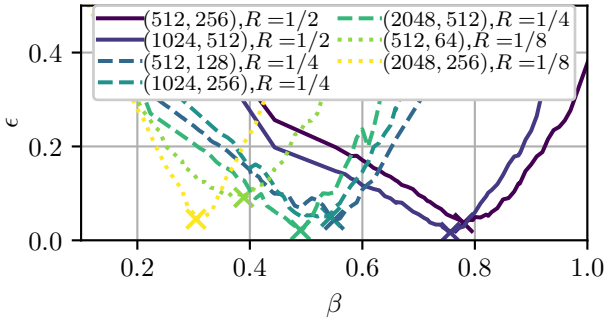

Fig. 8. MIESM ϵ over β for different coderates, $M = 2$.

them here. We observe that lower coderates result in lower β_{opt}. Though, the exact results vary slightly depending on the codeword length N. We recognize a tendency for lower β_{opt} for growing N. The results indicate that ESM adjustment factors mainly depend on coderate and only slightly on the exact codeword length. We conclude that it is sufficient to conduct simulations for each coderate with one codeword size N and one constellation order M to find a suitable β_{opt}.

VI. Conclusion

In our work we showed that it is possible to use MIESM and EESM algorithms for link abstraction in short packet communication systems with polar codes and low FER. We conclude that a relative error measure is advantageous for low FER systems because it yields a better curve match for low FER compared to other measures. Furthermore, we discussed the influence of system parameters on optimal adjustment factors. With MIESM, we can identify representative optimal adjustment factors for several varying system parameters instead of one for each configuration. Thus, we conclude we can obtain faster link abstraction with MIESM.

Acknowledgment

This work was partly funded by the German ministry of education and research (BMBF) under grants 16KIS0263K (HiFlecs) and 16KIS0720 (TACNET).

References

[1] A. Osseiran, J. F. Monserrat, and P. Marsch, *5G Mobile and Wireless Communications Technology*, 1st ed. New York, NY, USA: Cambridge University Press, 2016.

[2] V. Bioglio, C. Condo, and I. Land, "Design of Polar Codes in 5G New Radio," pp. 1–9, 2018.

[3] G. P. Fettweis, "The tactile internet: Applications and challenges," *IEEE Vehicular Technology Magazine*, vol. 9, no. 1, pp. 64–70, 2014.

[4] S. Dietrich, G. May, O. Wetter, H. Heeren, and G. Fohler, "Performance indicators and use case analysis for wireless networks in factory automation," in *2017 22nd IEEE International Conference on Emerging Technologies and Factory Automation (ETFA)*, 2017.

[5] G. Pocovi, K. I. Pedersen, and P. Mogensen, "Joint Link Adaptation and Scheduling for 5G Ultra-Reliable Low-Latency Communications," *IEEE Access*, vol. 6, pp. 28 912–28 922, 2018.

[6] I. Latif, F. Kaltenberger, and R. Knopp, "Link abstraction for multi-user MIMO in LTE using interference-aware receiver," in *IEEE Wireless Communications and Networking Conference, WCNC*. Shanghai, China: IEEE, 2012. [Online]. Available: https://ieeexplore.ieee.org/document/6214489/

[7] E. Arıkan, "Channel polarization: A method for constructing capacity-achieving codes for symmetric binary-input memoryless channels," *IEEE Transactions on Information Theory*, 2009.

[8] I. Tal and A. Vardy, "List Decoding of Polar Codes," *IEEE Transactions on Information Theory*, 2015.

[9] P. Giard, G. Sarkis, C. Leroux, C. Thibeault, and W. J. Gross, "Low-Latency Software Polar Decoders," 2015.

[10] H. Vangala, E. Viterbo, and Y. Hong, "A Comparative Study of Polar Code Constructions for the AWGN Channel," *arXiv*, 2015. [Online]. Available: https://arxiv.org/pdf/1501.02473.pdf

[11] K. Niu, K. Chen, and J. R. Lin, "Beyond turbo codes: Rate-compatible punctured polar codes," in *IEEE International Conference on Communications*, 2013.

[12] L. Zhang, Z. Zhang, X. Wang, Q. Yu, and Y. Chen, "On the puncturing patterns for punctured polar codes," in *IEEE International Symposium on Information Theory - Proceedings*, 2014.

[13] V. Bioglio, F. Gabry, and I. Land, "Low-Complexity Puncturing and Shortening of Polar Codes," in *2017 IEEE Wireless Communications and Networking Conference Workshops, WCNCW 2017*, 2017, pp. 0–5.

[14] A. Bravo-Santos, "Polar codes for the rayleigh fading channel," *IEEE Communications Letters*, vol. 17, no. 12, pp. 2352–2355, 2013.

[15] J. G. Proakis, *Digital Communications*, 3rd ed. McGraw-Hill, 1995.

[16] G. Caire, G. Taricco, and E. Biglieri, "Bit-Interleaved Coded Modulation," *IEEE Transactions on Information Theory*, vol. 44, no. 3, pp. 927–946, 1998.

[17] T. Richardson and R. Urbanke, *Modern Coding Theory*. New York, NY, USA: Cambridge University Press, 2008.

[18] G. Sarkis, I. Tal, P. Giard, A. Vardy, C. Thibeault, and W. J. Gross, "Flexible and low-complexity encoding and decoding of systematic polar codes," *IEEE Transactions on Communications*, 2016.

[19] P. Giard, "High-Speed Decoders for Polar Codes," Ph.D. dissertation, McGill University, Montreal, Canada, 2016. [Online]. Available: http://digitool.library.mcgill.ca/R/-?func=dbin-jump-full{&}object{_}id=145447

[20] E. Arikan, "Systematic polar coding," *IEEE Communications Letters*, 2011.

[21] H. Vangala, Y. Hong, and E. Viterbo, "Efficient algorithms for systematic polar encoding," *IEEE Communications Letters*, 2016.

[22] T. S. Rappaport, *Wireless Communications*, 2nd ed. Upper Saddle River, NJ, USA: Prentice Hall PTR, 2009.

[23] K. Brueninghaus, D. Astely, T. Salzer, S. Visuri, A. Alexiou, S. Karger, and G. Seraji, "Link Performance Models for System Level Simulations of Broadband Radio Access Systems," in *IEEE 16th International Symposium on Personal, Indoor and Mobile Radio Communications*, 2005.

[24] C. Bockelmann, *Robust Link Adaption in Coded OFDM Systems*. Aachen: Shaker Verlag, 2012.

[25] P. Jäckel, "A note on multivariate Gauss-Hermite quadrature," no. May, pp. 1–5, 2005. [Online]. Available: https://pdfs.semanticscholar.org/0e39/32b776eb3803e0f0ae2e414f69399daa411d.pdf